The Reaction Probability of OH on Organic Surfaces of Tropospheric Interest

Allan K. Bertram, Andrey V. Ivanov, Martin Hunter, Luisa T. Molina, and Mario J. Molina*

Department of Earth, Atmospheric and Planetary Sciences and of Chemistry, Massachusetts Institute of Technology, Cambridge, Massachusetts 02139

Received: April 16, 2001; In Final Form: July 24, 2001

Using a flow-tube reactor coupled to a chemical ionization mass spectrometer, we investigated the heterogeneous loss of OH on Halocarbon wax, two types of organized organic monolayers, and several solid organic surfaces (paraffin wax, stearic acid−palmitic acid mixture, pyrene, and soot) that are representative of surfaces found in the troposphere. The heterogeneous reaction is very efficient: the reaction probability is greater than 0.1 for all the organic surfaces investigated, except for Halocarbon wax. These results indicate that OH-organic heterogeneous reactions will significantly modify the hygroscopic properties and cloud condensation nuclei (CCN) ability of organic surfaces in the troposphere, and thus may play an important role in the Earth's radiative balance by affecting the properties of clouds. We also determined the diffusion coefficient of OH in helium to be 665 ± 35 Torr cm^2 s^{-1}. This value is close to that of its polar analogue, H_2O, suggesting that the diffusion coefficient of OH can be calculated accurately with H_2O transport properties.

1. Introduction

Organic carbon (OC) is a major component of fine particulate matter in the troposphere. In metropolitan U. S. areas, for example, high concentrations of condensed-phase OC are observed (5−20 $\mu g/m^3$), accounting for 15−60% by mass of particulate matter less than 10 μm in diameter (PM_{10}).[1] Over remote and rural U. S. sites, condensed-phase OC concentrations are substantially lower (<4 $\mu g/m^3$) but still comprise a major fraction of the total aerosol load (30−50% by mass of PM_{10}).[1] Particulate organic carbon can be either emitted directly into the atmosphere (primary OC) or formed in situ by the photooxidation of hydrocarbons (secondary OC).[2] The principal anthropogenic sources of condensed-phase organic material are fossil fuel use and biomass burning, and the principal natural source is emission from vegetation.[3] Fieldwork has shown that the composition of condensed-phase organic material is extremely complex, with hundreds of different organic compounds being identified.[4,5]

Heterogeneous reactions between OH and condensed-phase OC are of interest because these reactions may be responsible for the oxidation of organic aerosols in the atmosphere.[6] As a result, these reactions may modify the hygroscopic properties and cloud condensation nuclei (CCN) activity of organic aerosols.

Reactions between OH and gas-phase organic species have been studied extensively.[7,8] In most cases, these reactions are very fast, and accordingly, OH is the main oxidant of volatile organic species in the troposphere. In contrast, reactions between OH and condensed-phase organic material have received little attention, and thus, the rates and products of these reactions are essentially unknown. Initial studies, however, suggest that OH can react efficiently on organic surfaces. Jech et al.[9] determined that the reaction probability of OH on a malonic acid surface is greater than 0.1, and Cooper and Abbatt[10] showed that OH loss on ice surfaces is significantly enhanced in the presence of 1-hexanol (reaction probability > 0.2), which suggests that OH reacts efficiently with adsorbed 1-hexanol.

In the following, we present results from studies of the heterogeneous loss of OH on organic surfaces of tropospheric interest. The organic surfaces studied were organized organic monolayers (methyl- and vinyl-terminated monolayers), pyrene, paraffin wax (a mixture of *n*-alkanes), a stearic acid−palmitic acid mixture, and methane-soot. Soot, which is composed of both organic carbon and elemental carbon, was studied because it makes up a large fraction of the condensed-phase carbon in the troposphere. Organized organic monolayers were chosen because they provide well-defined surfaces for study[11] and because it has been suggested that a variety of atmospheric aerosols may be covered with a similar layer.[6,12] The remaining organics were chosen because they are often a relatively large fraction of the tropospheric fine particulate mass and because they represent several of the organic classes found in tropospheric particulate matter (polycyclic aromatic hydrocarbons, alkanes, and carboxylic acids).[5]

2. Experimental Section

2.1 Flow Tube Technique. The apparatus used in this work was similar to that previously used in our laboratory to study heterogeneous loss processes.[13] It consisted of a coated wall flow tube reactor coupled to a chemical ionization mass spectrometer (see Figure 1). The flow tube, 2.5 cm i.d. by 25 cm long, was constructed of borosilicate glass and included a movable injector through which OH was introduced. Helium, the main carrier gas, was introduced through a port at the upstream end of the flow reactor. All flow rates were determined with calibrated electronic mass flow meters (Tylan General) or by monitoring the rate of change of pressure in a known volume. The reactor pressure was monitored by a 0−10 Torr pressure gauge (MKS Baratron). Low pressures (1.0−1.5 Torr) were used when measuring reaction probabilities, and higher pressures (2−10 Torr) were used when measuring the diffusion coefficient of OH (see below). The average flow velocity in the reactor ranged from 1000 to 4000 cm s^{-1}, and the Reynolds number

* To whom correspondence should be addressed.

10.1021/jp0114034 CCC: $20.00
Published on Web 09/14/2001

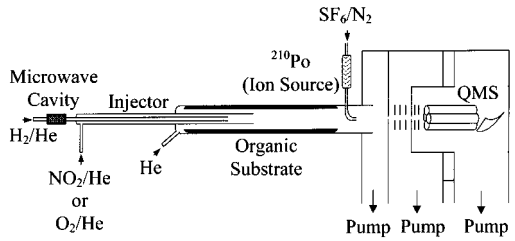

Figure 1. Schematic of experimental apparatus.

was less than 20. Under these conditions, the flows were laminar, the entrance length (the distance required to develop a parabolic velocity profile) was less than 2.5 cm, and the mixing distance (distance required for diffusion to reduce a radial concentration inhomogeneity to 5% of its initial value) was less than 3.0 cm.[14]

2.2 Radical Production. Two different methods were used to generate OH radicals. The first method consisted of generating OH radicals in the movable injector by the following fast reaction ($k_1 = 1.3 \times 10^{-10}$ cm^3 molecule^{-1} s^{-1}):[15]

$$H + NO_2 \rightarrow OH + NO \quad (1)$$

H atoms (10^9-10^{11} molecule cm^{-3} in the injector) were generated by passing a dilute mixture of molecular hydrogen in helium through an Evenson microwave cavity operating at 15−75 W. The H atoms were then combined with an excess of NO_2 (concentration in the injector ranged from approximately $10^{12}-10^{13}$ molecule cm^{-3}) 2 cm before the end of the injector. The reaction time in the final section of the injector (5−20 ms) was sufficient for practically all the H atoms to be converted to OH radicals. The OH signal was calibrated by introducing a known amount of NO_2 into the injector and by monitoring both the NO_2 signal and the OH signal with and without the microwave discharge on.

The second method consisted of the following reactions:

$$H + O_2 + M \rightarrow HO_2 + M \quad (2)$$

$$H + HO_2 \rightarrow 2OH \quad (3)$$

The rate constants for reactions 2 and 3 are 2.8×10^{-14} cm^3 molecule^{-1} s^{-1} (at 15 Torr) and 8.1×10^{-11} cm^3 molecule^{-1} s^{-1}, respectively.[15] Hydrogen atoms were generated in the microwave discharge and then combined with O_2 approximately 2 cm before the end of the injector. The pressure in the injector reaction zone was approximately 15 Torr in these experiments. Under these conditions, the ratio of [OH] to [HO_2] produced from this source was greater than 20.

2.3 Detection Method. OH, NO_2, and HO_2 were detected by chemical ionization mass spectrometry (CIMS) with SF_6^- as the reagent ion. SF_6^- was generated by passing a 10 ppm mixture of SF_6 in N_2 through a radioactive polonium source (^{210}Po). This reagent ion flow was added to the main flow through a sidearm located approximately 12 cm before the exit of the flow tube reactor. Both OH and NO_2 underwent charge-transfer reactions with SF_6^-:

$$OH + SF_6^- \rightarrow OH^- + SF_6 \quad (4)$$

$$NO_2 + SF_6^- \rightarrow NO_2^- + SF_6 \quad (5)$$

The rate constant for reaction 4 has been estimated to be 2×10^{-9} cm^3 molecule^{-1} s^{-1},[16] and the rate constant for reaction 5 is 1.4×10^{-10} cm^3 molecule^{-1} s^{-1}.[17] HO_2 was detected as $SF_4O_2^-$ after undergoing presumably a multistep reaction with SF_6^-.[18] The reaction time in the ion−molecule region was several milliseconds. At the end of the ion−molecule region, the ions were sampled through a 500-micron pinhole biased at approximately −15 V, focused with ion optics, and detected with a quadrupole mass spectrometer (QMS). The QMS was housed in a vacuum system that was differentially pumped by two turbo molecular pumps. The detection limit (a signal-to-noise of 1 with a 5 s integration time) for OH, HO_2, and NO_2 using this setup was 10^6, 10^7, and 10^7 molecule cm^{-3}, respectively, at 3.0 Torr.

2.4 Gases and Chemicals. Commercially available gases were used in these experiments: He (99.999%, BOC), N_2 (99.998%, BOC), SF_6 (99.99%, Matheson), and NO_2 (99.5%, Matheson). The gases that passed through the microwave discharge were further purified to avoid production of atomic impurities. Helium was first passed through an inert gas purifier (Aeronex, model 35 K) to remove traces of H_2, O_2, and H_2O, and hydrogen was passed though an oxygen-removing purifier (BOC, series 6210) and then through a liquid N_2 trap to remove H_2O.

The following organics were used in these studies: pyrene (98%, Aldrich), a stearic acid−palmitic acid mixture (43.2% stearic acid and 52.1% palmitic acid, Mallinckrodt), and paraffin wax (melting range 346−353 K, Aldrich). Halocarbon wax, an inert surface, was also used in some experiments to ensure that loss of OH by gas-phase reactions was minor (see discuss below); both the 600 series and the 1500 series were used. These organic materials are all solid at room temperature.

Octadecyltrichlorosilane, $CH_3(CH_2)_{17}SiCl_3$ (Aldrich, > 90%), and allyltrichlorosilane, $C_3H_5SiCl_3$ (Aldrich, 95%), were used to prepare the organic monolayers.

2.5 Surface Preparation. The inside wall of a Pyrex tube (1.9 cm i.d. and 20 cm in length) was coated with the organic material of interest and then inserted into the flow tube reactor. This coating provided the surface for the heterogeneous reactions.

Paraffin wax and Halocarbon wax films were prepared by melting the solid material, covering the inside of the Pyrex tube with the resulting liquid, and then letting the liquid solidify. Profilometry, transmission optical microscopy, and electron microscopy were used to characterize the films. The characterization measurements were performed using Pyrex slides rather than Pyrex tubes. The slides were prepared using the same techniques that were used to prepare the tubes. Profilometer measurements were carried out with a Tencor 10 Profiler equipped with a 2 μm stylus. Transmission optical microscope measurements were performed with Zeiss Axioskop 20 microscope equipped with 10× and 40× objectives, and electron microscope measurements were carried out with a XL30 environmental scanning electron microscope (Philips). Shown in Figure 2a, 2b, and 2c is an optical microscope image, an electron microscope image, and a profilometer scan of a paraffin wax film. Similar results were obtained for the Halocarbon wax films. The profilometer measurements indicate that the surface area of these films deviated from the surface area of the glass substrate by less than 5%, suggesting the films were smooth. The optical microscope and electron microscope images confirmed that the films prepared with this technique were smooth, nonporous, and completely covered the glass substrate. The thickness of the Halocarbon and paraffin wax films prepared with this technique ranged from approximately 5 to 75 μm.

Pyrene films were prepared by briefly dipping a Pyrex tube into a beaker of melted pyrene. A solid film of pyrene rapidly

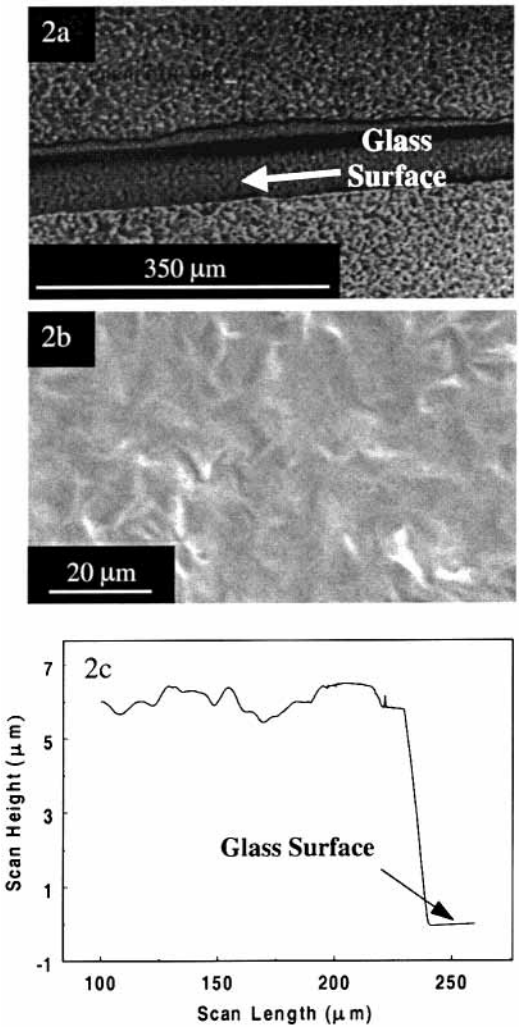

Figure 2. Optical microscope image (a), electron microscope image (b), and profilometer scan (c) of a paraffin wax film prepared with a melting technique. The glass substrate was exposed in 2a and 2c by scratching the wax film with a razor blade. The scratch shows the contrast between the wax film and the glass substrate.

crystallized on the Pyrex tube once it was removed from the melt. Stearic acid−palmitic acid films were prepared by first briefly dipping a Pyrex tube into a beaker of melted stearic acid and palmitic acid. This resulted in a liquid film on the Pyrex tube. Then the tube was briefly dipped in liquid nitrogen to induce rapid crystallization (otherwise, the liquid would drip off the tube before crystallization occurred). Shown in Figure 3a and 3b are electron microscope images of pyrene and stearic acid−palmitic acid films prepared with these techniques. Profilometer measurements of these surfaces indicate that the surface area of the pyrene and stearic acid−palmitic acid films deviated from the surface area of the glass substrate by approximately 10% and 6%, respectively. The 10% deviation for pyrene, however, is likely a lower limit since the profilometer measurements underestimate surface areas when the width of grooves and cracks is less than the depth of the grooves and cracks, which appears to be the case for our pyrene surfaces. The thickness of the pyrene and stearic acid−palmitic acid films prepared ranged from approximately 500 to 700 μm.

Soot surfaces were prepared by exposing the inner wall of the Pyrex tube to a methane flame, produced with a standard torch. Air entrained in the flame provided the oxidant for the flame (no additional oxygen was added to the torch). Figure 4, a microscope image of a soot surface prepared with this

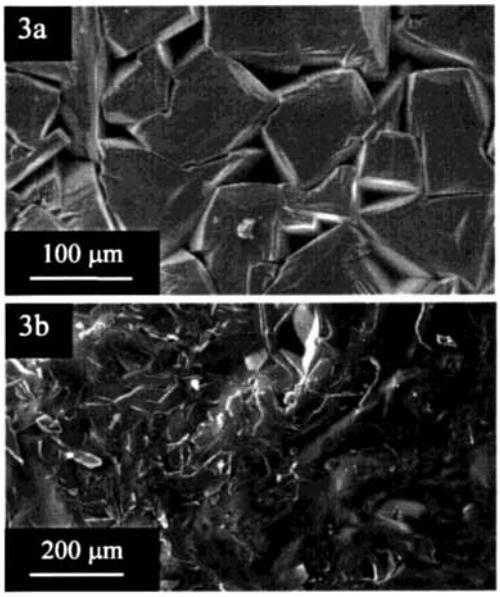

Figure 3. Electron microscope images of a typical pyrene film (a) and a stearic acid−palmitic acid film (b) used in our experiments.

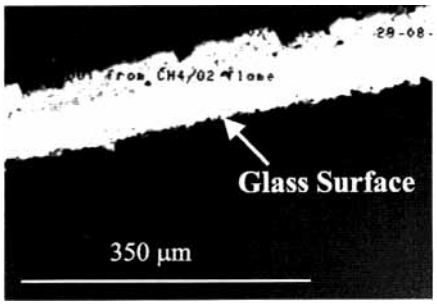

Figure 4. Optical microscope image of a soot surface prepared with a methane flame. The glass substrate was exposed by scratching the soot surface with a razor blade.

technique, shows that the soot formed a uniform coating on the glass substrate. The electron microscope images of the soot surface looked similar to the microscope images (no additional features were discernible). We were unable to determine the thickness of the soot film using profilometry, since the profilometer stylus scratched the film surface.

Organic monolayers were prepared using the self-assembly technique.[19] Vinyl-terminated ($-CH{=}CH_2$) and methyl-terminated ($-CH_3$) monolayers were prepared by treating Pyrex tubes with solutions of allyltrichlorosilane and octadecyltrichlorosilane, respectively. The contact angle between water droplets and the surface of the organic films was measured to verify the quality of the films. For the methyl- and vinyl-terminated monolayers, the contact angles were $100 \pm 2°$ and $95 \pm 2°$, respectively.

We also investigated the heterogeneous loss of OH on an aluminum oxide (alumina) surface because this surface proved to be convenient for measuring the diffusion coefficient of OH (see section 3.1 for further details). A tube constructed of aluminum was first rinsed with ethanol and then inserted directly into the flow tube reactor without removing the oxidized surface film.

3. Results and Discussion

Determination of the reaction probability, γ, consisted of the following steps: First, the OH signal was measured as a function of reaction time at low pressures (1.0−1.5 Torr). Then, from a

plot of ln(OH signal) versus reaction time, the observed first-order loss rate coefficient, k_{obs}, was determined. Next, the first-order wall loss rate coefficient, k_w, was calculated from k_{obs} using the Brown formalism,[20] which corrects for gas-phase diffusion of OH. Finally, gamma was calculated directly from k_w using the following equation:

$$\gamma = \frac{2rk_w}{c_{avg} + rk_w} \tag{6}$$

where c_{avg} is the average thermal velocity (cm s^{-1}) and r is the radius of the flow tube insert (cm). This equation takes into account that a concentration gradient will result in a net velocity component directed toward the surface.[21−23]

In the above data analysis, the diffusion coefficient of OH in He (D_{OH-He}) is required, and in addition, D_{OH-He} must be known accurately, since a large uncertainty in the diffusion coefficient can result in a large uncertainty in γ.[10,24] D_{OH-He} has been determined experimentally to be 600 ± 250 Torr cm^2 s^{-1},[25] but the uncertainty in this diffusion coefficient precludes the use of this value in our data analysis. Because the required transport properties of OH in He are not available, D_{OH-He} cannot be calculated from first principles with certainty. In the past, researchers have circumvented this problem by using a semiempirical formula, based on the diffusion coefficient of O atoms in He, to calculate D_{OH-He}.[26] However, this method may not be accurate if the diffusion coefficient of atomic oxygen is significantly different than D_{OH-He}. To reduce the uncertainty in the OH diffusion coefficient and thus reduce the uncertainty in our experimentally determined reaction probabilities, we have measured D_{OH-He} directly using the same apparatus used to measure the reaction probability.

3.1 Diffusion Coefficient Measurements. Determination of the diffusion coefficient was based on the rule of additivity of kinetic resistances:[13,27,28]

$$\frac{1}{k_{obs}} = \left(\frac{r^2}{3.66D_p}\right)P + \frac{1}{k_w} \tag{7}$$

where P is the pressure (Torr), r is the radius of the flow tube reactor (cm), and D_p is the diffusion coefficient (Torr cm^2 s^{-1}). According to this equation, a plot of $1/k_{obs}$ versus pressure gives a straight line with the slope inversely proportional to the diffusion coefficient. Determination of the diffusion coefficient using Equation 7 is appropriate if the reaction probability is close to unity, which is the case in these experiments (see below).

We have measured k_{obs} as a function of pressure on an alumina surface and on several of the organic surfaces. Shown in Figure 5, are typical results from these measurements. A total of 15 experiments were performed, resulting in 15 different plots of $1/k_{obs}$ versus pressure. From these plots, a diffusion coefficient of 665 ± 35 Torr cm^2 s^{-1} was determined. The diffusion coefficient determined with an alumina surface was within the uncertainty of the diffusion coefficient determined with the organic surfaces, confirming that the measured diffusion coefficient is independent of the surface.

The diffusion coefficient of O atoms based on three experimental studies is approximately 780 Torr cm^2 s^{-1}.[29−31] Our results indicate that the diffusion coefficient of OH is approximately 20% less than the diffusion coefficient of its nonpolar analogue, O. On the other hand, the diffusion coefficient of OH is very similar to the diffusion coefficient of H_2O, which is approximately 660 Torr cm^2 s^{-1}, based on two experimental studies.[32,33] This finding is in qualitative agreement with previous studies that showed that the diffusion coefficient of HO_2 is less than its nonpolar analogue, O_2, but similar to the diffusion coefficient of its polar analogue, H_2O_2.[34] On the basis of these findings, we suggest that the diffusion coefficient of OH in other gases, such as air, can be calculated accurately using H_2O transport properties, rather than transport properties of O atoms.

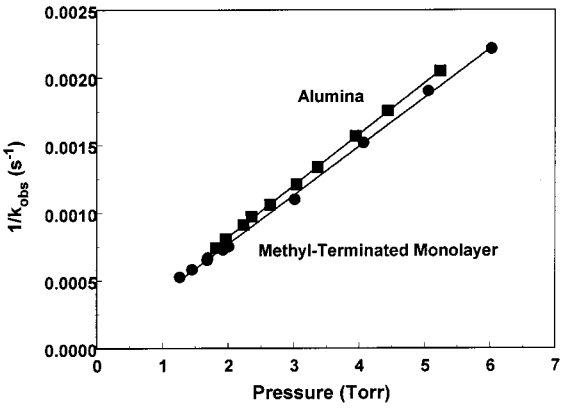

Figure 5. Inverse of the observed rate coefficient plotted as a function of the total flow tube pressure for two different surfaces: alumina and a methyl-terminated monolayer. The solid lines are the result of a linear least-squares fit to the data.

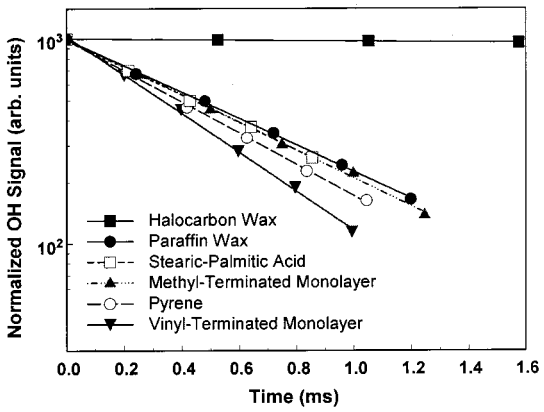

Figure 6. Plots of the OH signal versus reaction time. All experiments were performed at room temperature and approximately 1.25 Torr.

3.2 Results From Reaction Probability Measurements. The OH signal as a function of heterogeneous reaction time was measured for all the organic surfaces at approximately 1.25 Torr. Shown in Figure 6 are typical data from these studies. For all the organics, the OH signal decreases significantly with reaction time, but for Halocarbon wax, (solid squares in Figure 6) the OH signal remains practically unchanged. From the OH decays, we determined reaction probabilities as described above. The results are displayed in Table 1. γ_{OH}(avg) represents the average reaction probability, calculated using the average k_{obs} and the average D_{OH-He}. γ_{OH}(min) and γ_{OH}(max) represent the lower and upper limits to the average reaction probability. These upper and lower limits take into account both the uncertainty in D_{OH-He} and the uncertainty in k_{obs}. In most cases, the two uncertainties were comparable.

As expected, the reaction probability of OH on Halocarbon wax was small: the value was less than 1×10^{-3}, which is in agreement with previous measurements of OH loss on Halocarbon wax.[35,36] In contrast, the reaction probabilities of OH on organic surfaces were large, greater than 0.1. We also measured the reaction probability of OH on an alumina surface

TABLE 1: The Reaction Probability of OH Radicals, γ_{OH}, on Organic Surfaces and an Alumina Surface, Measured at Room Temperature

surface	γ_{OH}(avg)[a]	γ_{OH}(min)[b]	γ_{OH}(max)[b]
Halocarbon wax	6×10^{-4}	3×10^{-4}	9×10^{-4}
paraffin wax	0.34	0.16	1
methyl-terminated monolayer	0.29	0.14	1
stearic−palmitic acid	0.32	0.14	1
vinyl-terminated monolayer	0.60	0.25	1
pyrene	0.32	0.15	1
soot	0.88	0.50	1
Al_2O_3	0.20	0.11	0.44

[a] γ_{OH}(avg) represents the average reaction probability determined in our experiments. [b] γ_{OH}(min) and γ_{OH}(max) represent the lower and upper limits to the average reaction probability. The lower and upper limits take into account both the uncertainty in the OH diffusion coefficient and the uncertainty in the observed first-order loss rate coefficient, k_{obs}.

(see Table 1), obtaining results in agreement with previous studies.[25] Because small concentrations of OH (typically 1×10^8 molecule cm^{-3}) and short exposure times (<5 min) were used when determining the reaction probabilities listed in Table 1, only a small percentage (<10%) of surface sites potentially undergo reactions during the measurements (see section 4). Therefore, these reaction probabilities correspond to OH reactions on essentially "fresh" (unreacted) organic surfaces.

As discussed previously, the reaction probabilities presented in Table 1 were determined by first measuring k_{obs} at low pressures and then calculating k_w from k_{obs} using the Brown formalism. Alternatively, k_w can be determined by measuring k_{obs} as a function of pressure and calculating k_w from the intercept of a plot of $1/k_{obs}$ versus pressure (see eq 7).[13,27] For several of the organic surfaces, we determined the reaction probabilities using both methods, obtaining the same results within experimental error.

The reaction probabilities shown in Table 1 were determined by assuming that the surface area of the organic was equal to the geometric surface area. This assumption is reasonable for all the films except for soot and perhaps pyrene. Hence, the reaction probability for these two surfaces is an upper limit to the true reaction probability. Nevertheless, the correction factor for porous films is typically small (between 1/3 and 1) when the observed reaction probability is greater than 0.1.[37,38]

For pyrene and the stearic acid−palmitic acid mixture, the homogeneous OH-organic gas-phase reaction contributed less than 1% to the total loss of OH in our experiments. This was calculated using the vapor pressures of the organic materials[12,39] and the rate coefficients[40,41] of the OH-organic gas-phase reactions. (The gas-phase rate coefficients for stearic acid and palmitic acid were estimated using a semiempirical formula that is based on a structure−reactivity relationship.)[41] The vapor pressure of paraffin wax is unknown, so we measured directly the loss of OH due to the gas phase reaction between OH and paraffin wax vapor. This was measured by saturating the carrier gas with paraffin wax vapor and then by measuring the loss of OH due to the reaction with the vapor. In these experiments, the surface was coated with Halocarbon wax. Since the Halocarbon surface is basically unreactive, any loss of OH was attributed to the gas-phase reaction between OH and paraffin wax vapor. Using this method, we determined that the contribution of the gas-phase reaction with paraffin wax vapor was also less than 1% of the total OH loss due to the heterogeneous reaction with the paraffin wax surface.

As mentioned previously, we used two different sources to generate OH ($H + NO_2$ and $H + O_2 + M$). Within experimental uncertainty, we obtain the same results regardless of the source used, indicating our results are independent of the method used to generate OH. We also investigated the dependence of the reaction probability on OH and NO_2 concentrations. We measured k_{obs} on a methyl-terminated monolayer using OH concentrations ranging from 10^8 to 10^{10} molecule cm^{-3} and NO_2 concentrations ranging from 0 to 10^{11} molecule cm^{-3}. (The experiment that corresponds to $[NO_2] = 0$ molecule cm^{-3} was performed in excess of H atoms in the injector, and as a result, all the NO_2 was converted to OH and NO before entering the flow tube.) For all these experiments, k_{obs} varied by less than 5%, indicating that the measured reaction probability was independent of NO_2 and OH concentrations for the range studied.

TABLE 2: Comparison of Heterogeneous Loss (R_{Het}) to the Loss of OH by the Reaction with NO_2 (R_{NO2}) for Three Scenarios

environment	NO_2 (ppb)	surface area (cm^2 cm^{-3})	R_{Het}/R_{NO2}
urban	100	1.1×10^{-5}	0.004
rural	1	1.4×10^{-6}	0.04
remote	0.05	1.2×10^{-7}	0.08

3.3 Possible Mechanisms. Initial research indicates that the mechanisms responsible for organic surface reactions can be predicted reasonably well from the analogous gas-phase chemistry.[42,43] Accordingly, we can suggest the likely mechanisms responsible for OH loss in our experiments on the basis of known gas-phase chemistry. For example, the OH radical likely abstracted a H atom from the surfaces consisting of mainly long-chain alkanes (paraffin wax, methyl-terminated monolayer (C_{18}), and stearic acid−palmitic acid mixture) to form H_2O and a surface alkyl radical. Then, in the experiments that utilized the $H + NO_2$ source, OH, NO, or NO_2 probably added to the surface alkyl radical. In the experiments that utilized the $H + O_2 + M$ source, however, O_2 probably added to the surface alkyl radical to form a surface peroxy radical.[40]

If these mechanisms are correct, the surface of the organics will be oxidized by OH reactions and, hence, become more hydrophilic. To test this, we exposed the methyl-terminated monolayer to OH radicals for approximately 1 h, and then we determined the contact angle with water. (The $H + NO_2$ reaction was used to produce the OH radicals, and the OH concentration was 5×10^9 molecule cm^{-3}.) After exposure, the contact angle was 10°, compared to 100° before exposure. In contrast, when the methyl-terminated monolayer was exposed to just NO_2 (no OH) for 1 h, the contact angle did not change. Because the contact angle decreases as the surface becomes more hydrophilic, this preliminary experiment suggests that the organic surface is efficiently oxidized by OH heterogeneous reactions. In contrast, the reaction mechanism on an alumina surface is most likely catalytic, involving radical recombination.[9] Further studies in our laboratory will focus on the change in surface properties with exposure time and on the mechanisms of heterogeneous loss.

4. Possible Atmospheric Implications

Our results show that OH reacts very efficiently on organic surfaces of tropospheric interest; nevertheless, this is only of minor importance as a sink of OH in the troposphere since it does not compete with other loss processes of OH. To illustrate this point, we compared the rate of heterogeneous loss of OH by reactions with organic aerosols (R_{Het}) to the rate of homogeneous loss of OH by reactions with NO_2 (R_{NO2}) for typical tropospheric conditions (see Table 2). R_{NO2} values were calculated using NO_2 concentrations of 0.05, 1, and 100 ppm,

which correspond to remote, rural, and urban scenarios, respectively.[40,44−46] Heterogeneous loss rates were calculated using the following equation:[47]

$$R_{\mathrm{Het}} = \frac{c\gamma}{4} A[OH] \tag{8}$$

where c represents the mean thermal velocity of OH (cm s^{-1}), A represents the aerosol surface area (cm^2 cm^{-3}), γ represents the heterogeneous reaction probability, and $[OH]$ represents the OH concentration (molecule cm^{-3}). A reaction probability of 0.5, which is consistent with our experimental data, was used in these calculations. Typical aerosol surface areas in urban and rural areas were determined from the size parameters and particle number densities given by Jaenicke.[48] These surface areas correspond to the total aerosol, and hence they represent upper limits to the surface areas of organic particles. For the remote region, an organic aerosol content of 1500 cm^{-3} with an average diameter of 0.05 μm was assumed, on the basis of observations of organic particles in the marine environment by Novakov and Penner.[49] Equation 8 does not take into account gas-phase diffusion limitations, which are of minor importance for tropospheric aerosols with sizes less than 0.5 μm. For particles with sizes greater than approximately 0.5 μm, this equation overestimates the heterogeneous loss rate.

As seen from Table 2, the rate of heterogeneous loss of OH by reactions with organic aerosols is significantly less than the rate of homogeneous loss of OH by reactions with NO_2 for tropospheric conditions. Furthermore, this simple analysis does not consider other possible homogeneous loss processes of OH such as reactions with CO and CH_4, which can dominate in rural and remote regions when NO_2 concentrations are low.[50] Accordingly, heterogeneous loss of OH is of minor importance for typical tropospheric conditions.

On the other hand, OH heterogeneous reactions may play an important role in the atmosphere by initiating a sequence of radical reactions that leads to the oxidation of organic particles,[6] as discussed in section 3.3. The overall reaction mechanisms will differ slightly, however, from the reaction mechanisms discussed in section 3.3, because O_2, NO, and NO_2 are all present simultaneously in the atmosphere. As an example, if OH abstracts a H atom from a saturated aliphatic surface in the atmosphere to form a surface alkyl radical, molecular oxygen will probably add to the alkyl radical to form a surface alkyl peroxy radical. Next, NO or NO_2 may add to this surface radical, or NO may react with this surface radical to form NO_2 and a surface alkoxy radical.

Assuming the rate-limiting reaction for the oxidation of the surface to be the OH reaction, we have calculated the time required for the surface of an organic particle to be oxidized using our measured OH reaction probabilities and the following equation:

$$\text{Fraction of Surface Unoxidized} = \exp\left(-\frac{\gamma_0 Z t}{N_{\mathrm{total}}}\right) \tag{9}$$

where γ_0 represents the reaction probability of OH on an unreacted organic surface, Z represents the collision frequency of OH with the surface (molecule cm^{-2} s^{-1}), t represents time (s), and N_{total} represents the total number of surface sites available for reaction (reactive sites cm^{-2}). For these calculations, we assumed $N_{\mathrm{total}} = 1 \times 10^{15}$ reactive sites cm^{-2} and $\gamma_0 = 0.5$. Equation 9 was derived by assuming that the reaction probability is proportional to the fraction of surface sites unreacted. This equation, similar to eq 8, does not take into account gas-phase diffusion; nevertheless, gas-phase diffusion is of minor importance for tropospheric particles with sizes less than 0.5 μm, as indicated previously. For aerosols with sizes greater than 0.5 μm, this equation underestimates the time required for oxidation.

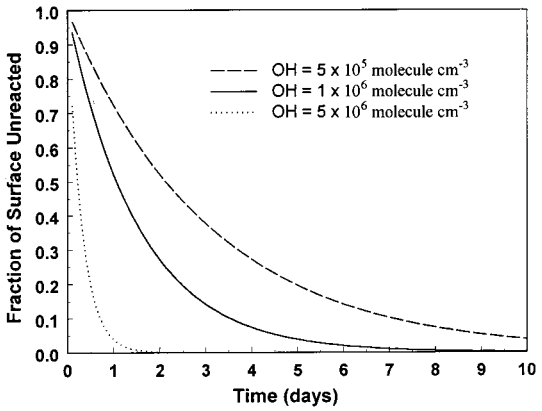

Figure 7. The fraction of an organic surface unreacted as a function of time in the troposphere, based on Equation 9 and the OH reaction probabilities determined in our studies. The three curves correspond to three different OH concentrations in the troposphere: a globally averaged OH concentration (1×10^6 molecule cm^{-3}) and approximate upper and lower limits to this global average (5×10^5 and 5×10^6 molecule cm^{-3}).

Shown in Figure 7 are the results of these calculations. The three curves in the figure correspond to three different OH concentrations in the atmosphere: a globally averaged OH concentration (1×10^6 molecule cm^{-3})[51] and approximate upper and lower limits to this global average (5×10^5 and 5×10^6 molecule cm^{-3}). The time for 90% of an organic surface to be oxidized for all three OH concentrations is less than 7 days. If the total number of surface sites available for reaction, N_{total}, is less than 1×10^{15} reactive sites cm^{-2}, then the time required for oxidation will be even shorter. For example, if N_{total} is 5×10^{14} reactive sites cm^{-2} and the OH concentration is 1×10^6 molecule cm^{-3}, 90% of the surface will be oxidized in less than 2 days.

The residence time of aerosols in the troposphere is estimated to be 5−15 days, on the basis of a global three-dimensional simulation of ^{210}Pb.[52] This residence time is comparable to the time required for oxidation of organic surfaces (Figure 7), which suggests that a significant fraction of the organic particles in the atmosphere will have oxidized surfaces. This conclusion agrees with previous suggestions by Ellison et al.[6] Because oxidized surfaces are hydrophilic, a significant fraction of the organic particles in the troposphere will have hydrophilic surfaces.

In the above discussion, we have assumed that organic particles in the atmosphere are solid and that only the surface of solid organic particles participates in heterogeneous reactions. Yet some organic particles may be partially or totally liquid.[53,54] In this case, all of the condensed-phase organic material, not just organics at the surface, may be potentially oxidized by heterogeneous reactions. Also, under certain conditions organic aerosols grow by condensation of organic vapors;[2] in this case, a new surface will be continuously available for oxidation. We suggest that atmospheric organic particles (solid, liquid, or growing) are efficiently oxidized by heterogeneous reactions and that these heterogeneous reactions may modify the hygroscopic properties and the CCN activity of organic aerosols.

5. Summary and Conclusions

The diffusion coefficient of OH in He was experimentally determined to be 665 ± 35 Torr cm^2 s^{-1}. This value is close to its polar analogue, H_2O, suggesting that the diffusion coefficient of OH can be calculated accurately with H_2O transport properties. The reaction probabilities of OH on solid organic surfaces and organized organic monolayers were investigated for the first time. The reaction probability for these organic surfaces (paraffin wax, organized organic monolayers, and stearic acid−palmitic acid mixture) is greater than 0.1. Preliminary results indicate that the organic surfaces are oxidized by these heterogeneous reactions. Experiments are currently underway in our laboratory to quantify this oxidation process and to determine the mechanisms and products of these reactions. We also measured the heterogeneous loss of OH on a methane-soot surface. These studies indicate that OH reacts efficiently on soot surfaces ($\gamma > 0.5$); however, more studies of this reaction are required to investigate, for example, the effect of surface porosity and the type of soot.[55,56] Finally, we have shown that OH-organic heterogeneous reactions may modify the hygroscopic properties and CCN ability of organic surfaces in the troposphere, and hence, may play an important role in the Earth's radiative balance by affecting the properties of clouds.

Acknowledgment. This work was supported by grants from the National Science Foundation and the U.S. Air Force Office of Scientific Research. We thank S. Trakhtenberg for help preparing the organized organic monolayers and for performing the contact angle measurements, and we thank Y. Gershenzon for helpful comments on the manuscript. A.K.B. thanks the Natural Science and Engineering Research Council of Canada for a Postdoctoral Fellowship. This work also made use of MRSEC shared facilities supported by the National Science Foundation under award number DMR-9400334 and NSF Laser Facility grant number 9708265-CHE.

References and Notes

(1) *Air Quality Criteria for Particulate Matter;* United States Environmental Protection Agency, EPA/600/P-95/001, 1996.

(2) Pandis, S. N.; Harley, R. A.; Cass, G. R.; Seinfeld, J. H. *Atmos. Environ.* **1992**, *26A*, 2269.

(3) Liousse, C.; Penner, J. E.; Chuang, C.; Walton, J. J.; Eddleman, H.; Cachier, H. *J. Geophys. Res.* **1996**, *101*, 19411.

(4) Rogge, W. F.; Mazurek, M. A.; Hildemann, L. M.; Cass, G. R.; Simoneit, B. R. T. *Atmos. Environ.* **1993**, *27A*, 1309.

(5) Seinfeld, J. H.; Pandis, S. N. *Atmospheric Chemistry and Physics*; Wiley-Interscience: New York, 1998.

(6) Ellison, G. B.; Tuck, A. F.; Vaida, V. *J. Geophys. Res.* **1999**, *104*, 11633.

(7) Atkinson, R. *Atmos. Environ.* **2000**, *34*, 2063.

(8) Atkinson, R.; Baulch, D. L.; Cox, R. A.; Hampson, R. F.; Kerr, J. A.; Rossi, M. J.; Troe, J. *J. Phys. Chem. Ref. Data* **1999**, *28*, 191.

(9) Jech, D. D.; Easley, P. G.; Krieger, B. B. In *Heterogeneous Atmospheric Chemistry*; Schryer, D. R., Ed.; American Geophysical Union: Washington, D. C., 1982; p 107.

(10) Cooper, P. L.; Abbatt, J. P. D. *J. Phys. Chem.* **1996**, *100*, 2249.

(11) Moise, T.; Rudich, Y. *J. Geophys. Res.* **2000**, *105*, 14667.

(12) Gill, P. S.; Graedel, T. E.; Weschler, C. *J. Rev. Geophys.* **1983**, *21*, 903.

(13) Poschl, U.; Canagaratna, M.; Jayne, J. T.; Molina, L. T.; Worsnop, D. R.; Kolb, C. E.; Molina, M. J. *J. Phys. Chem. A* **1998**, *102*, 10082.

(14) Keyser, L. F. *J. Phys. Chem.* **1984**, *88*, 4750.

(15) DeMore, W. B.; Sander, S. P.; Howard, C. J.; Ravishankara, A. R.; Golden, D. M.; Kolb, C. E.; Hampson, R. F.; Kurylo, M. J.; Molina, M. J.; *Chemical Kinetics and Photochemical Data for Use in Stratospheric Modeling*, Evaluation Number 12; JPL Publication 97-4; NASA Jet Propulsion Laboratory: Pasadena, 1997.

(16) Lovejoy, E. R.; Murrells, T. P.; Ravishankara, A. R.; Howard, C. J. *J. Phys. Chem.* **1990**, *94*, 2386.

(17) Huey, L. G.; Hanson, D. R.; Howard, C. J. *J. Phys. Chem.* **1995**, *99*, 5001.

(18) Elrod, M. J.; Meads, R. F.; Lipson, J. B.; Seeley, J. V.; Molina, M. J. *J. Phys. Chem.* **1996**, *100*, 5808.

(19) Sagiv, J. *J. Am. Chem. Soc.* **1980**, *102*, 92.

(20) Brown, R. L. *J. Res. Natl. Bur. Stand.* **1978**, *83*, 1.

(21) Semenoff, N. N. *Acta Physicochimica U. R. S. S.* **1943**, *18*, 1.

(22) Davison, B. *Proc. Phys. Soc.* **1951**, *64*, 881.

(23) Motz, H.; Wise, H. *J. Chem. Phys.* **1960**, *32*, 1893.

(24) Hanson, D. R.; Burkholder, J. B.; Howard, C. J.; Ravishankara, A. R. *J. Phys. Chem.* **1992**, *96*, 4979.

(25) Gershenzon, Y. M.; Ivanov, A. V.; Kucheryavyi, S. I.; Rozenshtein, V. B. *Kinet. Katal.* **1986**, *27*, 923.

(26) Marrero, T. R.; Mason, E. A. *J. Phys. Chem. Ref. Data* **1972**, *1*, 3.

(27) Zasypkin, A. Y.; Grigorieva, V. M.; Korchak, V. N.; Gershenson, Y. M. *Kinet. Katal.* **1997**, *38*, 772.

(28) Rudich, Y.; Talukdar, R. K.; Imamura, T.; Fox, R. W.; Ravishankara, A. R. *Chem. Phys. Lett.* **1996**, *261*, 467.

(29) Morgan, J. E.; Schiff, H. I. *Can. J. Chem.* **1964**, *42*, 2300.

(30) Judeikis, H. S.; Wun, M. *J. Chem. Phys.* **1978**, *68*, 4123.

(31) Plumb, I. C.; Ryan, K. R.; Barton, N. G. *Int. J. Chem. Kinet.* **1983**, *15*, 1081.

(32) Mason, E. A.; Monchick, L. *J. Chem. Phys.* **1962**, *36*, 2746.

(33) Schwertz, F. A.; Brow, J. E. *J. Chem. Phys.* **1951**, *19*, 640.

(34) Gershenzon, Y. M.; Grigorieva, V. M.; Ivanov, A. V.; Remorov, R. G. *Faraday Discuss.* **1995**, 83.

(35) Baulch, D. L.; Campbell, I. M.; Saunders, S. M. *J. Chem. Soc., Faraday Trans. 1* **1985**, *81*, 259.

(36) Ivanov, A. V.; Gershenzon, Y. M.; Gratpanche, F.; Devolder, P.; Sawerysyn, J. P. *Ann. Geophys.-Atmos. Hydrospheres Space Sci.* **1996**, *14*, 659.

(37) Leu, M. T.; Moore, S. B.; Keyser, L. F. *J. Phys. Chem.* **1991**, *95*, 7763.

(38) Keyser, L. F.; Moore, S. B.; Leu, M. T. *J. Phys. Chem.* **1991**, *95*, 5496.

(39) Sonnefeld, W. J.; Zoller, W. H.; May, W. E. *Anal. Chem.* **1983**, *55*, 275.

(40) Finlayson-Pitts, B. J.; Pitts, J. N., Jr. *Chemistry of the Upper and Lower Atmosphere*; Academic Press: Boston, 2000.

(41) Kwok, E. S. C.; Atkinson, R. *Atmos. Environ.* **1995**, *29*, 1685.

(42) Wadia, Y.; Tobias, D. J.; Stafford, R.; Finlayson-Pitts, B. J. *Langmuir* **2000**, *16*, 9321.

(43) Thomas, E. R.; Frost, G. J.; Rudich, Y. *J. Geophys. Res.* **2001**, *106*, 3045.

(44) National Research Council. *Rethinking the Ozone Problem in Urban and Regional Air Pollution*; National Academy Press: Washington, D. C., 1991.

(45) Emmons, L. K.; Carroll, M. A.; Hauglustaine, D. A.; Brasseur, G. P.; Atherton, C.; Penner, J.; Sillman, S.; Levy, H.; Rohrer, F.; Wauben, W. M. F.; VanVelthoven, P. F. J.; Wang, Y.; Jacob, D.; Bakwin, P.; Dickerson, R.; Doddridge, B.; Gerbig, C.; Honrath, R.; Hubler, G.; Jaffe, D.; Kondo, Y.; Munger, J. W.; Torres, A.; VolzThomas, A. *Atmos. Environ.* **1997**, *31*, 1851.

(46) Thakur, A. N.; Singh, H. B.; Mariani, P.; Chen, Y.; Wang, Y.; Jacob, D. J.; Brasseur, G.; Muller, J. F.; Lawrence, M. *Atmos. Environ.* **1999**, *33*, 1403.

(47) Ravishankara, A. R. *Science* **1997**, *276*, 1058.

(48) Jaenicke, R. In *Aerosol-Cloud-Climate Interactions*; Hobbs, P. V., Ed.; Academic Press: San Diego, CA, 1993.

(49) Novakov, T.; Penner, J. E. *Nature* **1993**, *365*, 823.

(50) Carslaw, N.; Creasey, D. J.; Heard, D. E.; Lewis, A. C.; McQuaid, J. B.; Pilling, M. J.; Monks, P. S.; Bandy, B. J.; Penkett, S. A. *J. Geophys. Res.* **1999**, *104*, 30241.

(51) Prinn, R.; Cunnold, D.; Simmonds, P.; Alyea, F.; Boldi, R.; Crawford, A.; Fraser, P.; Gutzler, D.; Hartley, D.; Rosen, R.; Rasmussen, R. *J. Geophys. Res.* **1992**, *97*, 2445.

(52) Balkanski, Y. J.; Jacob, D. J.; Gardner, G. M.; Graustein, W. C.; Turekian, K. K. *J. Geophys. Res.* **1993**, *98*, 20573.

(53) Feilberg, A.; Nielsen, T. *Environ. Sci. Technol.* **2000**, *34*, 789.

(54) Strommen, M. R.; Kamens, R. M. *Environ. Sci. Technol.* **1997**, *31*, 2983.

(55) Al-Abadleh, H. A.; Grassian, V. H. *J. Phys. Chem. A* **2000**, *104*, 11926.

(56) Stadler, D.; Rossi, M. J. *PCCP Phys. Chem. Chem. Phys.* **2000**, *2*, 5420.